Binderless Composite Electrode Monolith from Carbon Nanotube and Biomass Carbon Activated by KOH and CO_2 Gas for Supercapacitor

R. Farma[1,2], M. Deraman[1,*], R. Omar[1], Awitdrus[1,2], M. M. Ishak[1], E. Taer[1,2], and I.A. Talib[1]

[1] *School of Applied Physics, Faculty of Science and Technology, Universiti Kebangsaan Malaysia, 43600 Bangi, Selangor, Malaysia*

[2] *Department of Physics, Faculty of Mathematics and Natural Sciences, University of Riau, 28293 Pekanbaru, Riau, Indonesia*

[*] *Email: madra@pkrisc.cc.ukm.my*

Abstract. This paper presents a method to improve the performance of supercapacitors fabricated using binderless composite electrode monolith (BCMs) from self-adhesive carbon grains (SACG) of fibers from oil palm empty fruit bunches. The BCMs were prepared from green monoliths (GMs) contain SACG, SACG treated with KOH (5 % by weight) and SACG mixed with carbon nanotubes (CNTs) (5% by weight) and KOH (5 % by weight), respectively. These GMs were carbonized at 800°C under N_2 environment and activated by CO_2 gas at 800°C for 1 hour. It was found that addition of KOH and CNTs produced BCMs with higher specific capacitance and smaller internal resistance, respectively. It was also found that supercapacitor cells using these BCMs as electrodes exhibited a better specific energy and specific power. The physical properties of BCMs (density, electrical conductivity, porosity, interlayer spacing, crystallite dimension and microstructure) were affected by the addition of KOH and CNTs.

Keywords: BCMs, SACG, CNTs, BET surface area, supercapacitor, electrochemical properties
PACS: 82.45.Gj, 82.45.Mp, 82.45.Wx, 82.47.Uv, 82.45.Fk, 82.80.Fk, 81.05.uj, 81.05.U-, 81.05.Rm

INTRODUCTION

Supercapacitors are electrochemical storage devices whose range of energy and power densities can complement the function of batteries and dielectric capacitors to store energy and deliver power. Common type of supercapacitor electrodes are activated carbon [1,2], metal oxide [3,4] and electronically conducting polymer [5,6]. Activated carbon-based supercapacitors are widely developed because of their low cost, large capacitance and long cycling life. Electrostatic charges are stored at the activated carbon/electrolyte double layer interface and high capacitance can be achieved because of high specific surface area of the electrodes. However, activated carbon itself does not have a high enough electronic conductivity to ensure that supercapacitors would have a low equivalent series resistance (ESR) and hence lower energy or power loss during charging and discharging. Since carbon nanotube (CNTs) have high electronic conductivity, they have been used to improve the electrical conductivity of the electrodes by mixing them with activated carbon [7,8]. The specific capacitance of CNTs was found lower compared to activated carbon, therefore physical/chemical activation was used to increase their specific capacitance [9,10].

Here, we report the preparation and characterization of binderless composite electrode monoliths (BCMs) from self-adhesive carbon grains (SACG) of fibers of oil palm empty fruit bunches (EFB). In order to observe the effect of alkaline (KOH) treatment on the SACG toward the properties of BCMs, the BCMs were also prepared from the KOH treated SACG. Furthermore KOH treatment was also applied on the mixture of SACG and CNTs and the mixture was used to prepare BCMs. The effect of CNTs addition was investigated. CO_2 physical activation was carried out to produce BCMs. BCMs were characterized to investigate their density, electrical conductivity, porosity, microstructure and structure. The electrochemical behaviors of supercapacitor cells fabricated using these BCMs were investigated.

EXPERIMENTAL

Sample Preparation

SACG with particle size less than 106 microns were prepared from fiber of EFB by pre-carbonization

The 4th Nanoscience and Nanotechnology Symposium (NNS2011)
AIP Conf. Proc. 1415, 180-184 (2011); doi: 10.1063/1.3667251

(Furnace CTMSB46), milling for 36 hours (ball mill AC Motor BS 500-110) and sieving (Matest 24030 Brembate Sopra (BG)) [11]. A mixture of 28.5 g SACG and 1.5 g of KOH (5% by weight) was poured into 300 ml boiling water, stirred for 1 hour and followed by drying in an oven at 100°C for 48 hours. 10 g dried mixture were milled for 20 minutes to obtain homogeneous mixture of (SACG + KOH). A mixture of (90 % SACG + 5 % KOH + 5 % CNT, by weight) was also prepared using similar steps processes. 0.75 g SACG and mixtures inside a mould with a diameter of 20 mm, respectively, were converted into the green monoliths (GM1, GM2 and GM3) by a press pelletizing machine (VISITEC 2009-Malaysia).

The GMs were carbonized into carbon monoliths in a carbonization furnace (Vulcan Box Furnace 3-1750) under a 1.5 $l$min^{-1} flow of N_2 gas, up to 800°C, using our previous multi-step heating profile [11]. BCMs were produced from carbon monoliths by CO_2 (1.0 $l$min^{-1}) activation at 800°C for 1 hour with a heating rate of 5°C min^{-1}. After polished to a thickness of 0.4 mm, BCMs were used as electrodes in symmetrical supercapacitor cells using stainless steel 316L as current collector and H_2SO_4 (1 Molar) as electrolyte.

Characterization

The dimensions (Mitutoyo 193-253) and weight (Mettler Toledo. AB204) of the monoliths were measured to determine the density of the GMs and BCMs. A four-point-probe technique (Jandel Universal Probe & Keithley Micro-Ohmeter 220) was used to determine the electrical conductivity of the BCMs. Field Emission Scanning Electron Microscope (FESEM) (Zeiss SUPRA 55VP) was used to study the microstructures of the BCMs. X-ray diffractometer (Bruker AXS: model D8 Advance, wavelength of 1.5406 Å) was used to record the X-ray diffraction (XRD) pattern of the BCMs. The nitrogen (77 K) adsorption-desorption isotherm experiments (Micromeretic ASAP 2010) were conducted to characterize the porosity of the BCMs.

The performance of the supercapacitor cells using BCMs as their electrodes was studied by galvanostatic charge-discharge (GCD), electrochemical impedance spectroscopy (EIS) and cyclic voltammetry (CV) methods using an electrochemical instrument-interface (Solartron SI 1286 and Solartron 1255HF Frequency Respond Analyzer).

RESULTS AND DISCUSSION

The results in Table 1 clearly show that alkaline treatment and addition of CNTs into SACG precursor did contribute to the change in weight (w), thickness (t), diameter (d) and density (ρ) of the GMs and BCMs. The electrical conductivity (σ) of the BCMs is also affected by the alkaline treatment and addition of CNTs.

TABLE 1. Weight (g), dimension (mm) and density (gcm^{-3}) of GMs and BCMs, and electrical conductivity ((Ωmm)$^{-1}$) of BCMs

Samples	w	d	t	ρ	σ
GM1	0.732	20.153	2.286	1.004	-
GM2	0.735	20.156	2.206	1.045	-
GM3	0.725	20.133	2.183	1.034	-
BCM1	0.278	14.426	1.593	1.068	1.022
BCM2	0.272	14.253	1.513	1.127	1.290
BCM3	0.305	14.986	1.623	1.067	1.432

XRD data in Figure 1 show that all of the BCMs have a turbostratic structure [12-14], with major and minor peaks at 23.849° and 44.882° (BCM1), 23.670° and 44.204° (BCM2), 24.941° and 43.772° (BCM3) due to diffraction from (002) and (100) planes, respectively. The calculated values of interlayer spacing (d_{002} and d_{100}) and crystallite dimension (stack height L_c (002) and stack width L_a (100)) from the diffraction peaks (002) and (100) are shown in Table 2. The relationship between d, L, surface area and specific capacitance for carbon from EFB is reported in ref. [12].

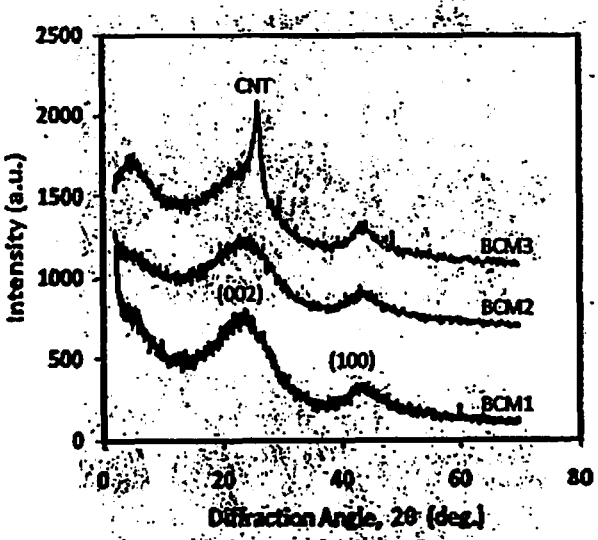

FIGURE 1. XRD pattern for BCMs.

TABLE 2. Interlayer spacing and crystallite dimension for BCMs

Samples	d_{002} (Å)	d_{100} (Å)	L_c (Å)	L_a (Å)
BCM1	3.7285	2.0181	9.03	51.07
BCM2	3.7539	2.0462	8.95	38.32
BCM3	3.5676	2.0667	12.45	57.17

Comparison of FESEM micrographs in Figures 2 (a) and (b) show that the BCM2 is more porous than BCM1, indicating the effect of alkaline treatment.

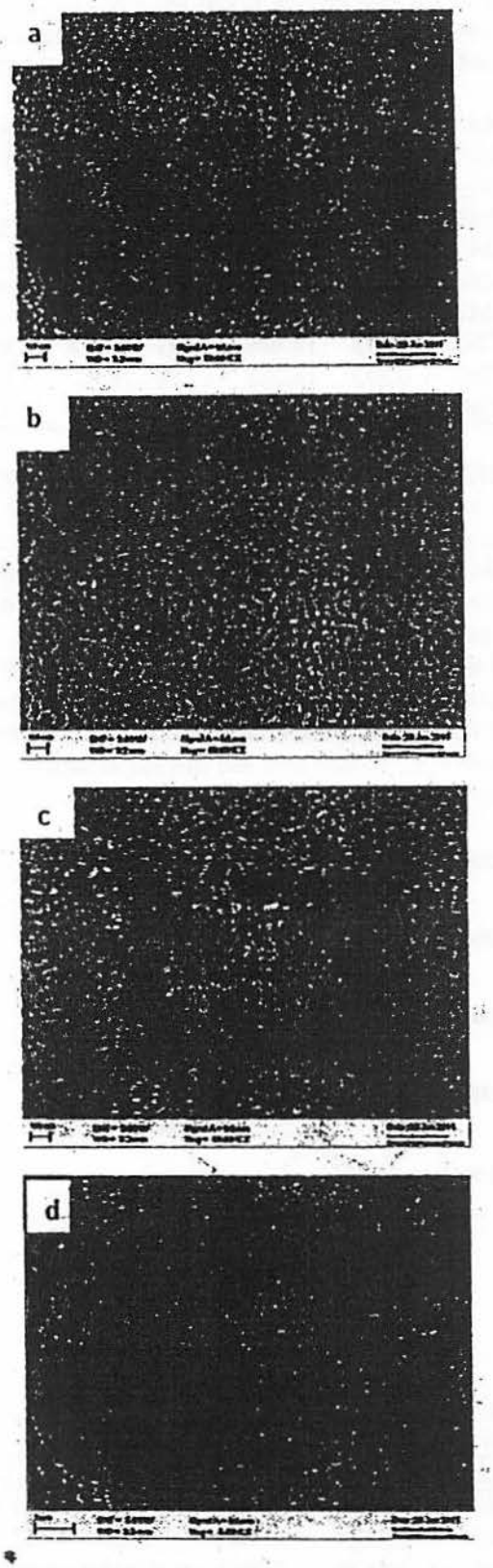

FIGURE 2. FESEM Micrographs for (a) BCM1, (b) BCM2, (c) BCM3, (d) CNTs in pores.

Porosity in BCM3 (Figure 2 (c)) is similar with that in BCM2, and however some of its pores are occupied by CNTs (Figure 2 (d)).

The plot of adsorption-desorption capacity versus pressure in Figure 3 show that all the BCMs have a typical type I isotherm. The values of pore parameters (Tables 3) obtained from Figure 3 show that alkaline treatment enhances the porosity of the BCMs. S_{BET} is the BET surface area, S_{Meso} and S_{Micro} are the surface area of mesopores and micropores, V_{Meso} and V_{Micro} are the volume of mesopores and micropores and D is the average pore diameter. Some pores that are occupied by CNTs reduce the surface area of the BCMs.

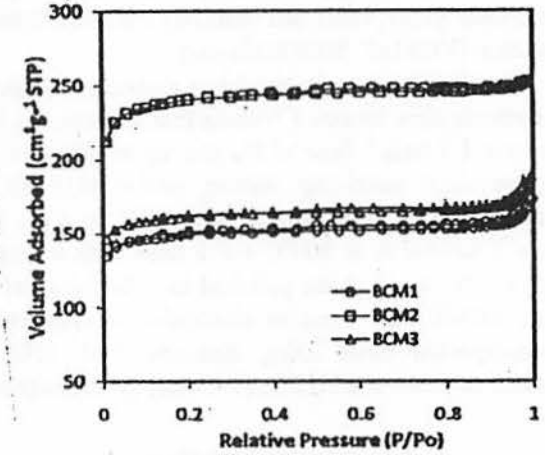

FIGURE 3. Adsorption-desorption capacity versus pressure for BCMs.

TABLE 3. Porosity data for BCMs

Samples	BCM1	BCM2	BCM3
S_{BET} (m^2g^{-1})	448	723	485
S_{Meso} (m^2g^{-1})	55	98	58
S_{Micro} (m^2g^{-1})	394	626	427
V_{Meso} (cm^3g^{-1})	0.0504	0.0599	0.0538
V_{Micro} (cm^3g^{-1})	0.2066	0.3284	0.2241
D (nm)	2.2943	2.1479	2.2903

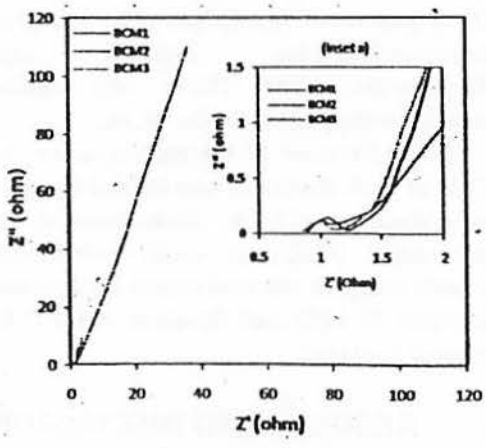

FIGURE 4. Nyquist plots for BCMs cells.

The Nyquist plots from EIS data in Figure 4 (inset a) clearly show their differences, indicating a significant

effect of the alkaline treatment in improving a supercapacitive performance of the cell. Table 4 compares the values of R_s, R_p, ESR, f_k and R_k of the three cells obtained from the EIS data in Figure 4. R_s (intercept of Z'' at Z' axis for high f region) is the resistances of electrolyte and contact between current collectors and electrodes, R_p (intercept of Z'' at Z' axis for low f region) is the internal resistance of electrode, ESR = (R_p-R_s), f_k is the knee frequency and R_k is the resistance corresponding to f_k. The specific capacitance was calculated from the EIS data using equation $C_{sp} = 2C_{cell}/m$, where $C_{cell} = -1/(2\pi fZ'')$, f is the frequency (lowest), Z'' is the imaginary part of impedance and m is the mass of electrode (Table 4) [16].

TABLE 4. The value of R_s, R_p, ESR, f_p, R_k for ACM cells

Cells	R_s (Ohm)	R_p (Ohm)	ESR (Ohm)	f_k (Hz)	R_k (Ohm)
BCM1	0.934	1.187	0.252	79.43	1.269
BCM2	0.711	1.772	1.061	01.58	1.361
BCM3	0.860	1.109	0.248	63.10	1.186

The GCD plots, shown in Figure 5, for the BCMs cells in the potential range of 0 – 1 V at the current densities of 10 $mAcm^{-2}$, show an almost linear behavior of charge-discharge curves. A sharp drop in voltage at the beginning of the discharge curves is associated with ESR of the supercapacitor cells. The specific capacitance was calculated (Table 5) from the discharge curve using equation $C_{sp} = (2I\Delta t)/(m\Delta V)$, where I is the discharge current, Δt is the discharge time, ΔV is the voltage, and m is the mass of electrode [16].

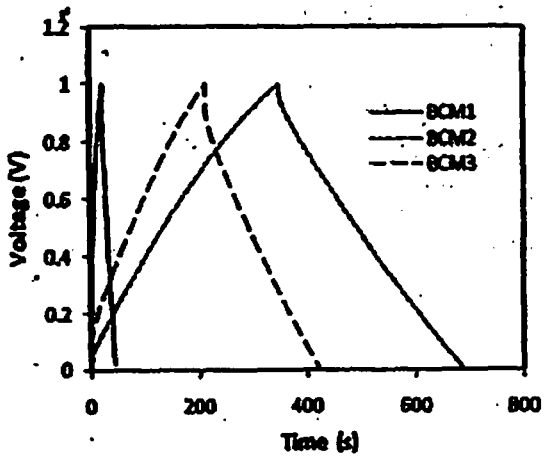

FIGURE 5. GCD curves for BCMs cells.

The increase in area of rectangular shape of CV curves for the BCMs cells, for the potential values from 0.1 V to 1.0 V at a scan rate of 1 mVs^{-1} (Figure 6), indicates the supercapacitive behavior of the cells gains improvement due to the alkaline treatment. A slight decrease in cell performance is observed with the addition CNTs. The specific capacitance was calculated (Table 5) from the CV data using equation $C_{sp} = 2I/(s\,m)$, where I is the current, s is the scan rate and m is the mass of electrode [17]. The values of C_{sp} calculated from the EIS, GCD and CV methods (Table 5) are different but they show a good trend of overall magnitude.

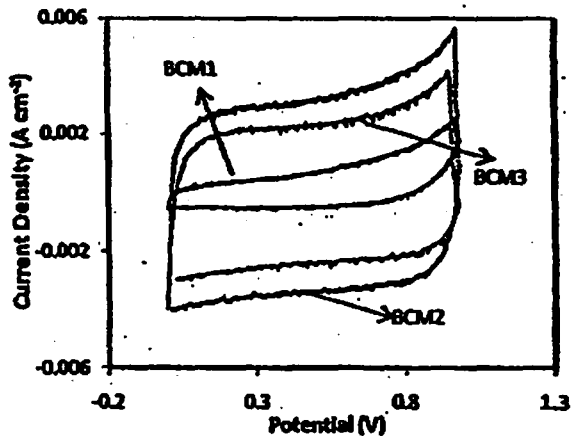

FIGURE 6. CV curves for BCMs cells.

TABLE 5. Specific capacitance (C_{sp}) for BCMs (x = EIS, y = CV, z = GCD)

Cells	$^{x}C_{sp}$ (Fg^{-1})	$^{y}C_{sp}$ (Fg^{-1})	$^{z}C_{sp}$ (Fg^{-1})
BCM1	4.8	18.3	7.5
BCM2	84.7	108.2	117.7
BCM3	56.3	77.7	76.1

The specific power (P) and specific energy (E) of BCMs cells were calculated from the GCD curves (Figure 5) using equations P = VI/m and E = VIt/m, respectively, where I is the discharge current, V is the voltage, t is time in hour and m is the mass of electrode [18,19,20]. Ragone plots, P versus E, in Figure 7 clearly show that BCM2 cell offers a much better P-E relationship than that of the BCM1 cell, indicating a significant role of

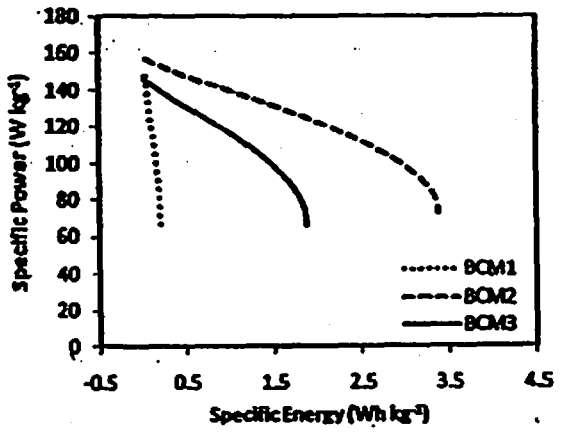

FIGURE 7. Ragone plots for BCMs cells.

alkaline treatment. Addition of CNTs causes the P-E curve for the BCM3 cell to be less satisfactory than that of the BCM2 cell but it is still significantly better than that of the BCM1 cells.

CONCLUSION

It was found that treatment of SACG from EFB by KOH at room temperature did help the CO_2 activation to produce BCMs with high porosity from these treated GMs precursors. Consequently, supercapacitor cells fabricated using these BCMs as their electrodes show better performance compared to that using BCMs from untreated SACG. Use of CNTs slightly reduces the porosity of BCMs and the cell performance but it can improve the ESR cell. The change in BCMs porosity due to the addition of KOH and CNTs is associated with the change in density, electrical conductivity, structure and microstructure of the BCMs.

ACKNOWLEDGMENT

The authors acknowledge the Fundamental Research Grant (UKM-ST-07-FRGS 0030-2009) for the project entitled "Study of Interface between Current Collector and Carbon Electrode Based on Biomass and Nanomaterials in Supercapacitor" and the UKM grant (UKM-OUP-NBT-29-145/2011).

REFERENCES

1. Y. Liu, Z. Hu, K. Xu, X. Zheng, Q. Gao, *Acta Phys. - Chim. Sin.*, 24, 1143–1148 (2008).
2. B. Xu, Y. Chen, G. Wei, G. Cao, H. Zhang and Y. Yang, *Mater. Chem. Phys.* 124, 504-509 (2010).
3. R.R. Salunkhe, K. Jang, H. Yu , S. Yu , T. Ganesh, S.-H. Han, H. Ahn, *J. Alloys Compd.* 509, 6677-6682 (2011).
4. V.D. Patake, S.M. Pawar, V.R. Shinde, T.P. Gujar, C.D. Lokhande, *Curr. Appl. Phys.* 10, 99-103 (2010).
5. K.-W. Chang, Z.-Y. Lim, F.-Y. Du, Y.-L. Yang, C.-H. Chang, C.-C. Hu, H.-P. Lin, *Diamond Relat. Mater.* 18, 448-451 (2009).
6. G.A. Snook, P. Kao, A.S. Best, *J. Power Sources* 196, 1-12 (2011).
7. P.-L. Taberna, G.C. Chevallier, P. Simon, D. Plee, T. Aubert, *Mater. Res. Bull.* 41, 478-484 (2006).
8. Q.-Y. Li, Z.-S. Li, L. Lin, X.Y. Wang, Y.-F. Wang, C.-H. Zhang, H.-Q. Wang, *Chem. Eng. J.* 156, 500-504 (2010).
9. C. Li, D. Wang, T. Liang, X.Wang, L.Ji, *Matt. Lett.* 58, 3774-3777 (2004).
10. J.M. Ko, K.M. Kim, *Mater. Chem Phys.* 114, 837-841 (2009).
11. M. Deraman, R. Omar, S. Zakaria, I.R. Mustapa, M. Talib, N. Alias, R. Jaafar, *J. Mater. Sci.* 3, 3329-3335 (2002).
12. Awitdrus, M. Deraman, I.A. Talib, R. Omar, M.H. Junali, E. Taer, M.M. Saman, *Sains Malaysiana* 39, 83-86 (2010).
13. A.R. Coutinho, J.D. Rocha, C.A. Luengo, *Fuel Process. Technol.* 67, 93–102 (2000).
14. M. Deraman, S.K.M. Saat, M.M. Ishak, Awitdrus, E. Taer, I.A. Talib, R. Omar, M.H. Junali, AIP Proceeding, *The 3rd Nanoscience and Nanotechnology Symposium* (NNSB2010), Bandung, Indonesia, 179-186 (2010).
15. D. Hulicova-Jurcakova, M. Seredych, Y. Jin, G.Q. Lu, T.J. Bandosz, *Carbon* 48, 1767-1778 (2010).
16. E. Taer, M. Deraman, I.A. Talib, A.A. Umar, M. Oyama, R.M. Yunus, *Curr. Appl. Phys.* 10, 1071-1075 (2010).
17. A.L.M. Reddy, M.M. Shaijumon, S.R. Gowda, P.M. Ajayan, *J. Phys. Chem.* C 114, 658-663 (2010).
18. A.S. Raut, C.B. Parker, J.T. Glass, *J. Mater. Res.* 25, 1500-1506 (2010).
19. E. Taer, M. Deraman, I.A. Talib, S.A. Hashmi, A.A. Umar, *Electrochim. Acta*, 56, 10217-10222 (2011).
20. E. Taer., M. Deraman, I.A. Talib, A. Awitdrus, S.A. Hashmi, A.A. Umar, *Int. J. Electrochem. Sci.* 6, 3301-3315 (2011).